Water Research 83 (2015) 161–170

Contents lists available at ScienceDirect

Water Research

journal homepage: www.elsevier.com/locate/watres

Modeling the low pH limit of *Nitrosomonas eutropha* in high-strength nitrogen wastewaters

Alexandra Fumasoli [a], Eberhard Morgenroth [a, b], Kai M. Udert [a, *]

[a] Eawag: Swiss Federal Institute of Aquatic Science and Technology, Überlandstrasse 133, 8600 Dübendorf, Switzerland
[b] Institute of Environmental Engineering, ETH Zürich, 8093 Zürich, Switzerland

ARTICLE INFO

Article history:
Received 10 March 2015
Received in revised form
13 May 2015
Accepted 8 June 2015
Available online 23 June 2015

Keywords:
Bioenergetics
Intracellular pH
Chemical speciation
Buffer intensity
Nitrifiers

ABSTRACT

In wastewater treatment, the rate of ammonia oxidation decreases with pH and stops very often slightly below a pH of 6. Free ammonia (NH_3) limitation, inhibition by nitrous acid (HNO_2), limitation by inorganic carbon or direct effect of high proton concentrations have been proposed to cause the rate decrease with pH as well as the cessation of ammonia oxidation. In this study, we compare an exponential pH term common for food microbiology with conventionally applied rate laws based on Monod-type kinetics for NH_3 limitation and non-competitive HNO_2 inhibition as well as sigmoidal pH functions to model the low pH limit of ammonia oxidizing bacteria (AOB). For this purpose we conducted well controlled batch experiments which were then simulated with a computer model. The results showed that kinetics based on NH_3 limitation and HNO_2 inhibition can explain the rate decrease of ammonia oxidation between pH 7 and 6, but fail in predicting the pH limit of *Nitrosomonas eutropha* at pH 5.4 and rates close to that limit. This is where the exponential pH term becomes important: this term decreases the rate of ammonia oxidation to zero, as the pH limit approaches. Previously proposed sigmoidal pH functions that affect large pH regions, however, led to an overestimation of the pH effect and could therefore not be applied successfully. We show that the proposed exponential pH term can be explained quantitatively with thermodynamic principles: at low pH values, the energy available from the proton motive force is too small for the NADH production in *Nitrosomonas eutropha* and related AOB causing an energy limited state of the bacterial cell. Hence, energy limitation and not inhibition or limitation of enzymes is responsible for the cessation of the AOB activity at low pH values.

1. Introduction

Ammonia oxidizing bacteria (AOB) release 2 moles of protons per mole of ammonia that is oxidized to nitrite. If the buffer capacity in the bulk solution is low, biological ammonia oxidation causes a substantial pH drop, which in turn affects the rate of ammonia oxidation. In wastewater treatment, ammonia oxidation decreases with pH and usually stops when the pH value drops below pH 6 (Painter, 1986). However, the reasons for the rate decrease, but especially for the cessation of activity are not very well understood. There are also some exceptions in wastewater treatment where AOB have adapted to low pH environments and grew at pH values as low as 4 (Gieseke et al., 2006) or even below (Udert et al., 2005).

The pH dependence and the pH limit of AOB is usually not relevant for conventional wastewater treatment as most municipal wastewaters contain sufficient alkalinity to allow complete ammonia oxidation (Tchobanoglous et al., 2003). However, the pH dependence of AOB becomes important in wastewaters with a low alkalinity to ammonia ratio, such as human urine (Udert et al., 2003a) or digester supernatant (Van Hulle et al., 2007).

The pH has a crucial role during nitrification of these wastewaters, because it influences AOB and nitrite-oxidizing bacteria (NOB) differently and thereby determines whether nitrite or nitrate is the main nitrification product. The SHARON (Single reactor High activity Ammonia Removal Over Nitrite) process for instance is deliberately operated at pH values above 7 and temperatures of 30°C (Hellinga et al., 1999), because under these conditions AOB grow faster than NOB causing the wash out of the latter. In contrast, NOB should be retained in nitrification reactors with urine, when nitrified urine is further processed to a fertilizer product (Udert et al., 2015). To ensure that NOB are retained in the system, this process is operated at pH values as low as 6 or even below (Etter

* Corresponding author.
E-mail address: kai.udert@eawag.ch (K.M. Udert).

http://dx.doi.org/10.1016/j.watres.2015.06.013

et al., 2013), where the growth rate of AOB is reduced strongly. Despite the low pH values, nitrite can accumulate in the system, which is a major problem for this process (Etter et al., 2013). Hence, a model that reliably predicts the rate of nitrite production by AOB at such low pH values would be of great benefit to understand and improve the process performance. Furthermore, as nitrite accumulation is usually a result of a dynamic change in the reactor pH (Etter et al., 2013), this model requires explicit pH calculations.

The growth rate of AOB decreases with pH, because at low pH values the actual substrate of AOB (Suzuki et al., 1974), NH_3 occurs only at very low concentrations even if the total ammonia (NH_4^+ and NH_3) concentration is high. AOB are also known to be inhibited by nitrous acid (HNO_2), the acid of their own product nitrite (NO_2^-) (Anthonisen et al., 1976). To account for the effects of NH_3 limitation and HNO_2 inhibition on the ammonia oxidation in digester supernatant, Hellinga et al. (1999) proposed a first kinetic expression. This rate law bases on a Monod term for NH_3 and a term for non-competitive inhibition by HNO_2.

Whereas Hellinga et al. (1999) were able to model their data by considering effects of NH_3 and HNO_2 only, Wett and Rauch (2003) found that limitation of total inorganic carbon (TIC) was the main reason for the decrease in ammonia oxidation at low pH values and that NH_3 limitation was often overestimated. TIC concentrations are generally low at low pH values, because its acid H_2CO_3 is formed, which volatilizes as CO_2 (pK_a value 6.35, Stumm and Morgan, 1996). According to their measurements, Wett and Rauch (2003) found that a sigmoidal term for bicarbonate (HCO_3^-) was suitable to account for the effects of TIC limitation.

Besides an indirect effect of pH via the speciation of NH_3/NH_4^+ and NO_2^-/HNO_2 and H_2CO_3/HCO_3^-, pH has been suggested to influence AOB directly (Antoniou et al., 1990; Van Hulle et al., 2007; Wiesmann et al., 2006). Wiesmann et al. (2006) explained the direct pH effect for nitrifiers with protein damage, but they did not propose a model to account for this inhibition. Van Hulle et al. (2007) proposed a bell-shaped curve to model the pH dependency of AOB in the SHARON process and explained the effect by an increased demand for maintenance energy and the effect of pH on the structure and permeability of the cell membrane. Finally, Antoniou et al. (1990) attributed the direct pH effect of AOB to the pH dependence of the rate limiting enzyme. They suggested that the controlling enzyme is only active in a certain ionization state, which was expressed with a sigmoidal pH term. However, Antoniou et al. (1990) applied this model between pH 6.4 and 8.5, but not to values close to the pH limit. Furthermore, they did not consider indirect pH effects (e.g., the effect of NH_3 limitation).

Models to predict the low pH limit of bacteria, however, were the main focus of many studies from food microbiology in order to prevent microbial growth in foods and to ensure food safety. Presser et al. (1997) proposed to multiply the growth rate with an exponential pH inhibition term to model the deactivation of *Escherichia coli* under acidic conditions (e.g., after lactic acid fermentation). This exponential pH term bases on the experimental observation that the growth rate is fairly constant over a wide pH range and decreases only as the pH limit is approached.

The pH term proposed by Presser et al. (1997) is based on an empirical observation and is not built on first principles. However, the exponential pH term resembles the rate law proposed by Jin and Bethke (2002, 2007), who proposed to extend conventional Monod-type kinetics with a thermodynamic potential factor. This factor approaches 1, when the thermodynamic driving force is large, but it decreases to zero as the driving force depletes. The thermodynamic driving force is the difference between the energy available and the energy required to drive a particular reaction. The synthesis of ATP as well as of NADH are important reactions for the energy metabolism of AOB (Poughon et al., 2001). The energy required to synthesize ATP or NADH is derived from the proton motive force (Nicholls and Ferguson, 1997), which is a transmembrane electrochemical gradient that results from the extrusion of protons from the cyto- to the periplasm during cellular respiration. Hence, the thermodynamic potential factor approaches zero, when the stored energy in the proton motive force is just enough to satisfy the energy requirements for ATP or NADH production.

Even though many studies focused on the pH influence on nitrifiers, only very few studies represent models that provide predictions of pH. The model by Hellinga et al. (1999) included pH calculations based on acid-base equilibria only. However, for a realistic modeling of pH in high strength wastewaters ion activity and complex formation have to be considered as well (Batstone et al., 2012). This is definitely the case for source-separated urine (Udert et al., 2003b). Accurate modeling of pH is a prerequisite for being able to predict the influence of low pH on nitrification.

In this study, we compared the exponential pH term from Presser et al. (1997) with commonly used mathematical expressions (Monod, non-competitive inhibition and sigmoidal pH dependency) to model the pH dependency and the low pH limit of AOB. The exponential pH term is explained quantitatively with bioenergetic calculations. The kinetic expressions were tested and compared with well-controlled batch experiments. To maximize the accuracy of the pH calculations, it was necessary to develop and validate a chemical speciation model, which includes ionic strength corrections and complex formation.

2. Experiments

2.1. Batch experiments

Batch experiments were conducted in a 2 L column reactor. The reactor was aerated with a constant air flux (1 $L \cdot min^{-1}$) controlled with a red-y GCR flowmeter (Vögtlin Instruments AG, Aesch, Switzerland). The air flux was chosen sufficiently high to enable good mixing conditions. Additionally the reactor was stirred magnetically at 500 rpm (RCT basic, Ika Labortechnik, Staufen, Germany). Shortly before the experiments, the Kaldnes® K1 biofilm carriers (0.75 L) were taken from an operating pilot scale reactor for urine nitrification (Section 2.4). The temperature was controlled at 25 ± 0.1°C with a thermostat (F32, Julabo Labortechnik GmbH, Seelbach, Germany). The oxygen concentration remained above 6.3 $mg \cdot L^{-1}$ in all experiments.

The initial pH value of the solution was adjusted to 7 by adding a one-molar sodium hydroxide solution. During the batch experiments, pH was not adjusted, such that the lower pH limit was reached. The experiments lasted for 12 h, except for two experiments (NH_4^+(a-b), Table 1), which lasted 22 h. These time durations were chosen to make sure that the low pH limit was clearly reached. Experiments NH_4^+(a-b) lasted longer, because the rate of

Table 1
Composition of the synthetic solutions at the beginning of the batch experiments.

	NH_4–N $mg \cdot L^{-1}$	NO_2–N $mg \cdot L^{-1}$
NH_4^+(a)	35	0.7
NH_4^+(b)	69	1.0
NH_4^+(c)	145	0.8
NH_4^+(d)	333	2.1
NH_4^+(e)	1010	1.7
NO_2^-(a)	333	28.1
NO_2^-(b)	326	41.6
NO_2^-(c)	326	105
NO_2^-(d)	326	310
NO_2^-(e)	319	898

ammonia oxidation was slower, such that more time was required to reach the low pH limit. Samples were taken at constant time intervals until the pH limit was reached. Samples were immediately filtrated (0.45 μm, MN GF-5, Macherey–Nagel, Düren, Germany) and analyzed for total ammonia, total nitrite and nitrate. At the beginning and at the end of each batch experiment samples were taken to characterize the urine composition (for measured parameters see Table S1, supplementary information).

To investigate the influence of NH_3 we used five synthetic solutions (NH_4^+(a) to NH_4^+(e)) that contained initial total ammonia concentrations of 28, 42, 105, 310 and 1010 mg $N \cdot L^{-1}$. The total ammonia and total nitrite concentrations of the solutions at the beginning of the experiments are given in Table 1. The complete composition and the recipes for all synthetic solutions are given in Table S1 and S2 in the supplementary information. Nitrite was consumed by NOB during the experiments and was below the detection limit (0.1 mg $N \cdot L^{-1}$). Synthetic urine solutions were used, because this allowed us to freely vary total ammonia concentrations, which would not have been possible in real nitrified urine. We did not add nitrate to the synthetic urine solutions, as we aimed to follow the increase in nitrate during the experiments (not shown in this study) and the expected changes were too small to be detected with high background nitrate concentrations. To investigate the influence of HNO_2, we used five synthetic solutions (NO_2^-(a) to NO_2^-(e)) containing initial total nitrite concentrations of 28, 42, 105, 310 and 898 mg $N \cdot L^{-1}$ (Table 1 and Table S1, supplementary information). The total ammonia concentrations in these experiments were between 319 and 333 mg $N \cdot L^{-1}$. We also investigated the influence of nitrite in four experiments, where sodium nitrite was added to the effluent solution of a nitrification reactor operated with real urine (Etter et al., 2013). As the biodegradable organic substances are mostly degraded in the nitrification reactor, the real nitrified urine solutions contained hardly any biodegradable organic substances. The starting concentrations of total nitrite were between 50 and 208 mg $N \cdot L^{-1}$ and the total ammonia concentrations between 850 and 882 mg $N \cdot L^{-1}$, respectively (Real (a) to Real (d), Table S1, supplementary information). Furthermore, we investigated the pH limit in one experiment with suspended sludge in a real nitrified urine solution. This experiment was performed to see whether the model is directly applicable to a suspended sludge system (Suspended, Table S1, supplementary information).

To investigate the influence of TIC, different gas mixtures were used to achieve a CO_2 partial pressure of 0, 5 and 10%. Synthetic air containing 20% O_2 and 80% N_2 was used for experiments without CO_2. Synthetic air with 10% CO_2, 18% O_2 and 72% N_2 was used for a partial CO_2 pressure of 10%. The two types of synthetic air were mixed with red-y GCR flowmeters (Vögtlin Instruments AG, Aesch, Switzerland) to obtain the CO_2 partial pressure at 5%. The synthetic and real nitrified urine solutions for the three experiment CO_2(a) to CO_2(c) contained total ammonia concentrations between 801 and 996 mg $N \cdot L^{-1}$ (Table S1, supplementary information) and total nitrite was mostly oxidized to nitrate (NO_3^-) by NOB during the experiments.

2.2. Titration

Titrations were performed to validate the chemical speciation model and to test which degree of complexity (ionic strength effects, number of complexation reactions) would be required. The pH range for titration was 4–8.5. We conducted the titration experiments in synthetic urine solutions (Table S1, supplementary information). The reactor contained 1 L of the solution. The initial pH of the solution was adjusted to pH 4. The pH was then increased by dosing a 1 mol $\cdot L^{-1}$ sodium hydroxide solution. The reactor was stirred magnetically at approximately 500 rpm and temperature was controlled at 25 ± 0.1°C. To prevent CO_2 uptake from ambient air due to stirring, the headspace was flushed with N_2 gas during titrations. To investigate the influence of biomass on the buffer intensity, we added 0.375 mL of well drained Kaldnes® K1 biofilm carriers (Section 2.4) to the synthetic solution. Before adding the biofilm carriers to the reactor, they were washed three times with the same solution that was used for titration.

2.3. Analytical methods

Chloride, sulfate, phosphate, nitrate, potassium and sodium were analyzed with ion chromatography (IC, Metrohm, Herisau, Switzerland). Magnesium and calcium were determined with inductively coupled plasma optical emission spectrometry (ICP OES, Ciros, Spectro Analytical Instruments, Kleve, Germany). The total ammonia concentration was measured photometrically with cuvette tests (LCK 303, Hach-Lange, Berlin, Germany) or on a flow injection analyzer (FIA, Application Note 5220, FOSS, Hillerød, Denmark). Total nitrite was measured with FIA (Application Note 5200) or IC. TIC and total organic carbon (TOC) were measured with a TIC/TOC analyzer (IL550 OmniTOC, Hach-Lange, Berlin, Germany). The standard deviation for all measurements was below 4%.

To increase the accuracy of the pH data, we used 2 pH meters (pH-meter 605, Metrohm, Herisau, Switzerland) with two different pH electrodes (Sentix 41, WTW, Weilheim, Germany and 405-DXX-S8/225, Mettler-Toledo, Greifensee, Switzerland) for continuous pH measurement. The average of the two measurements was used for all calculations. The measurement of the two sensors differed maximally by 0.03 units. Both pH sensors were calibrated before each experiment in buffer solutions preheated to 25°C. O_2 was measured with a mobile WTW device (Oxi340, WTW, Weilheim, Germany). Temperature was measured with a Pt100 sensor (Pt100/4/Cl/.A, Endress & Hauser, Reinach, Switzerland). All data were recorded in 30 s intervals on a data logger (Memograph S, RSG40, Endress & Hauser, Reinach, Switzerland).

2.4. Pilot scale reactor and characterization of ammonia oxidizing population

The biomass for the batch experiments originated from a pilot scale nitrification reactor (Etter et al., 2013). During the phase of batch experiments, the pH in the pilot reactor was between 5.6 and 6.2. Amplicon pyrosequencing analyses of the floc and biofilm fractions of the biomass (not shown) revealed that most of the autotrophic biomass was attached to the carriers. The biofilm carriers and not the suspended sludge were therefore used in the batch experiments. The biofilm carriers were used since the attached biomass could not be removed from the carrier material without destroying it.

To characterize the ammonia oxidizing population, a sample of two biomass carriers was taken from the reactor and stored at −20°C prior to molecular analysis. Metagenomic DNA was extracted from the carriers using the FastDNA SPIN Kit for Soil (MP Biomedicals, Santa Ana, CA, USA) with adaptation to manufacturer's protocol, and analyzed by Research and Testing Laboratory (Lubbock, TX, USA) for bacterial tag-encoded FLX amplicon pyrosequencing (bTEFAP) according to in-house protocol (Sun et al., 2011) a primer pair targeting the v1-v3 hypervariable region of the bacterial 16S rRNA gene pool (27F/518R) (Weissbrodt et al., 2012). A total number of 28145 reads was obtained in the sequencing set. The denoised sequencing datasets were processed and mapped against the Greengenes database of reference 16S rRNA gene sequences (DeSantis et al., 2006) in the bioinformatics PyroTRF-ID workflow (Weissbrodt et al., 2012). The dominant

sequences related to AOB were then retrieved out of the PyroTRF-ID annotation files and aligned against NCBI BLASTn (Altschul et al., 1997) in order to validate the taxonomic assignments at identity level. The relative abundances of AOB in the overall bacterial community covered by the primer pair were calculated as the amount of reads mapping with reference sequences of AOB compared to the total sequencing depth.

3. Models

3.1. Nitrification model

In the computer model biological processes and gas exchange as well as acid-base equilibria and complex formation were implemented. To calculate the chemical speciation reactions, the effect of ionic strength was considered for charged species, which means that we calculated in activities and not in concentrations. Activity coefficients were estimated from ionic strength according to the Davies approach as described in Stumm and Morgan (1996).

The biological processes growth and decay of AOB and NOB were included in the model. The growth and decay of heterotrophic bacteria were neglected in the model to decrease the complexity of the model and as the content of biodegradable organic substances was negligible low (Table 1, supplementary information). The stoichiometric matrix is given in Table 2. The main focus of this study was on the kinetic expression for AOB. To model the growth of AOB we used three kinetic approaches:

- Model 1 includes Monod terms for NH_3 and HNO_2 only (Hellinga et al., 1999):

$$r_{AOB} = \mu_{max,AOB} \cdot \frac{\{NH_3\}}{\{NH_3\} + K_{NH3,AOB}} \cdot \frac{K_{I,\ HNO2,AOB}}{\{HNO_2\} + K_{I,\ HNO2,AOB}} \cdot X_{AOB} \quad (1)$$

where r_{AOB} is the rate of ammonia oxidation (g COD·L^{-1}·d^{-1}), μ_{max} the maximum growth rate (d^{-1}), $K_{NH3,AOB}$ the affinity constant for NH_3 (mol·L^{-1}), $K_{I,HNO2,AOB}$ the non-competitive inhibition constant for HNO_2 (mol·L^{-1}), and X_{AOB} the biomass concentration of AOB (g COD·L^{-1}). All constants are specified in Table 3.

- Model 2 is based on Monod terms for NH_3 and HNO_2 and a sigmoidal pH term (Antoniou et al., 1990; Jubany, 2007):

$$r_{AOB} = \mu_{max,AOB} \cdot \frac{\{NH_3\}}{\{NH_3\} + K_{NH3,AOB}} \cdot \frac{K_{I,\ HNO2,AOB}}{\{HNO_2\} + K_{I,\ HNO2,AOB}} \cdot \frac{1}{1 + \frac{10^{-pH}}{10^{-pK}}} \cdot X_{AOB} \quad (2)$$

where pK is the lower half saturation constant for pH (Antoniou et al., 1990; Jubany, 2007). The initial formula contains also an upper pK value for the enzyme inhibition at high pH values. However, for pH values below pH 7, this term can be neglected.

- Model 3 includes Monod terms for NH_3 and HNO_2 and an exponential pH term (Presser et al., 1997; Ratkowsky, 2002):

$$r_{AOB} = \begin{cases} 0, & pH < pH_{min} \\ \mu_{max,AOB} \cdot \frac{\{NH_3\}}{\{NH_3\} + K_{NH3,AOB}} \cdot \frac{K_{I,\ HNO2,AOB}}{\{HNO_2\} + K_{I,\ HNO2,AOB}} \cdot \left(1 - 10^{(K_{pH}(pH_{min} - pH))}\right) \cdot X_{AOB}, & pH \geq pH_{min} \end{cases} \quad (3)$$

where pH_{min} is the minimal pH for growth, and K_{pH} a fitting parameter.

For the growth of NOB we used Haldane kinetics as proposed by Hellinga et al. (1999), which was also applied in Jubany (2007):

$$r_{NOB} = \mu_{max,NOB} \cdot \frac{\{HNO_2\}}{\{HNO_2\} + K_{HNO2,NOB} + \frac{\{HNO_2\}^2}{K_{I,HNO2,NOB}}} \cdot X_{NOB} \quad (4)$$

where $K_{HNO2,NOB}$ and $K_{I,HNO2,NOB}$ are the affinity and inhibition constant for HNO_2 (mol·L^{-1}), respectively, and X_{NOB} the biomass concentration of NOB (g COD·L^{-1}).

Decay of AOB and NOB was modeled according to Jubany (2007):

$$r_{Decay} = b \cdot X \quad (5)$$

where r_{Decay} is the decay rate (g COD·L^{-1}·d^{-1}), and b the decay coefficient (d^{-1}).

The gas exchange of CO_2 due to bubble aeration was included in the model as follows:

Table 2
Stoichiometric matrix for bacterial growth and decay of AOB and NOB. The parameters are specified in Table 3.

Parameter	X_{AOB}	X_{NOB}	O_2	NH_3	HNO_2	NO_3	CO_2	H^+
	g COD	g COD	mol	mol	mol	mol	mol	mol
AOB								
Aerobic growth	1		$(1-48/Y_{AOB})/32$	$-1/Y_{AOB}-i_N$	$1/Y_{AOB}$		$-i_C$	
Decay	−1		−1/32	i_N			i_C	
NOB								
Aerobic growth		1	$(1-16/Y_{NOB})/32$	$-i_N$	$-1/Y_{NOB}$	$1/Y_{NOB}$	$-i_C$	$1/Y_{NOB}$
Decay		−1	−1/32	i_N			i_C	

Table 3
Kinetic parameter for microbial growth and decay of AOB and NOB included in the computer models.

Parameter		Value	Unit	Reference
Nitrogen fraction of biomass	i_N	0.00625	mol N·g COD^{-1}	Assumed composition of biomass: $C_5H_7O_2N$
Carbon fraction of biomass	i_C	0.03125	mol C·g COD^{-1}	
AOB				
Maximal growth rate	$\mu_{max,AOB}$	1.21	d^{-1}	Jubany (2007)
Decay rate	b_{AOB}	0.20	d^{-1}	Jubany (2007)
Growth yield	Y_{AOB}	2.52	g COD·mol N^{-1}	Jubany (2007)
NH_3 affinity constant	$K_{NH3,AOB}$	$5.36\cdot10^{-5}$	mol·L^{-1}	Van Hulle et al. (2007)
HNO_2 inhibition constant	$K_{I,HNO2,AOB}$	$1.46\cdot10^{-4}$	mol·L^{-1}	Van Hulle et al. (2007)
Constant (Model 2)	pK	6.78	–	Jubany (2007)
Constant (Model 3)	K_{pH}	2.3	–	Fitted
NOB				
Maximal growth rate	$\mu_{max,NOB}$	1.02	d^{-1}	Jubany (2007)
Decay rate	b_{NOB}	0.17	d^{-1}	Jubany (2007)
Growth yield	Y_{NOB}	1.12	g COD·mol N^{-1}	Jubany (2007)
HNO_2 affinity constant	$K_{HNO2,NOB}$	$1.70\cdot10^{-7}$	mol·L^{-1}	Jubany (2007)
HNO_2 inhibition constant	$K_{I,HNO2,NOB}$	$9.57\cdot10^{-6}$	mol·L^{-1}	Jubany (2007)

$$r_{CO_2} = H_{CO_2}\cdot(\{CO_2\} - \{CO_{2,Sat}\})\cdot\frac{Q_{gas}}{V}\cdot\left(1 - e^{\frac{-KLa_{CO2}\cdot V}{Q_{gas}\cdot H_{CO2}}}\right) \quad (6)$$

where r_{CO2} is the rate of CO_2 volatilization (mol·L^{-1}·d^{-1}), H_{CO2} the Henry coefficient for CO_2 (1.2 mol(g)·mol(aq)$^{-1}$, Stumm and Morgan 1996), $CO_{2,sat}$ the saturation concentration of CO_2 in the water phase in relation to the gas concentration in the inlet air (mol·L^{-1}, Section S2, supplementary information), Q_{gas} the controlled gas flow (L·d^{-1}), V the liquid volume (L), and K_La_{CO2} the gas exchange coefficient for CO_2 (d^{-1}). K_La_{CO2} was estimated from K_La_{O2} based on the penetration theory and the assumption that the diffusion coefficient for CO_2 is 20% smaller than that for O_2 (Section S2, supplementary information). The K_La_{O2} was estimated with experiments in deionized water with the same reactor configuration used for the batch experiments. NH_3 and HNO_2 volatilization were neglected, due to the low volatility and the low concentrations of both compounds.

Table 4
Acid-base equilibria and complex formation included in the computer models. All values are given for 25°C and zero ionic strength.

Equation	pK_a
Acid-Base equilibria	
$HCO_3^- \rightleftharpoons CO_3^{2-} + H^+$	10.33[a]
$H_2CO_3 \rightleftharpoons HCO_3^- + H^+$	6.35[a]
$NH_4^+ \rightleftharpoons NH_3 + H^+$	9.24[a]
$HNO_2 \rightleftharpoons NO_2^- + H^+$	3.25[b]
$H_3PO_4 \rightleftharpoons H_2PO_4^- + H^+$	2.15[a]
$H_2PO_4^- \rightleftharpoons HPO_4^{2-} + H^+$	7.20[a]
$HPO_4^{2-} \rightleftharpoons PO_4^{3-} + H^+$	12.38[a]
$HSO_4^- \rightleftharpoons SO_4^{2-} + H^+$	1.99[a]
$H_2O \rightleftharpoons OH^- + H^+$	14.00[a]
Complex formation	
$K^+ + H_2PO_4^- \rightleftharpoons KH_2PO_4$	−0.30[a]
$K^+ + H_2PO_4^- \rightleftharpoons KHPO_4^- + H^+$	6.30[a]
$2K^+ + H_2PO_4^- \rightleftharpoons K_2HPO_4 + H^+$	6.07[a]
$K^+ + SO_4^{2-} \rightleftharpoons KSO_4^-$	−0.85[a]
$Na^+ + H_2PO_4^- \rightleftharpoons NaH_2PO_4$	−0.30[a]
$Na^+ + H_2PO_4^- \rightleftharpoons NaHPO_4^- + H^+$	6.13[a]
$2Na^+ + H_2PO_4^- \rightleftharpoons Na_2HPO_4 + H^+$	6.25[a]
$Na^+ + SO_4^{2-} \rightleftharpoons NaSO_4^-$	−0.74[a]
$NH_4^+ + H_2PO_4^- \rightleftharpoons NH_4H_2PO_4$	−0.10[c]
$NH_4^+ + HPO_4^{2-} \rightleftharpoons NH_4HPO_4^-$	−1.30[c]
$NH_4^+ + SO_4^{2-} \rightleftharpoons NH_4SO_4^-$	−1.03[a]

[a] Thermo_minteq.dat, standard database in Visual MINTEQ (Gustafsson, 2012).
[b] Lide (2009).
[c] Smith et al. (2004).

The acid-base equilibria and complex formation reactions considered in the model are shown in Table 4. Chemical equilibria were modeled with back- and forward reactions (Udert et al., 2003b). As an example, equation (7) shows the rate expression of the NH_3/NH_4^+ equilibrium:

$$r_{NH_3} = -r_{NH_4^+} = k_{eqNH_3}\cdot\left(\left\{NH_4^+\right\} - \{NH_3\}\cdot\left\{H^+\right\}\cdot 10^{pK_{NH_3}}\right) \quad (7)$$

where r_{NH3} and r_{NH4+} are the rate of NH_3 and NH_4^+ production (mol·L^{-1}·d^{-1}), respectively, and k_{eqNH3} the rate constant for equilibrium (d^{-1}). The value of all equilibrium rate constants was 10^6 d^{-1} and thereby much larger than any other kinetic constant in the model.

The computer model was implemented in the simulation environment AQUASIM (Reichert, 1994). For parameter estimation, we used the secant algorithm implemented in AQUASIM. K_{pH} was the only fitted kinetic parameter. Furthermore, the initial AOB concentration (X_{AOB}) was fitted to the measured pH values and the initial NOB concentration (X_{NOB}) to the measured total nitrite concentrations for each experiment. The estimated parameters and the standard errors for K_{pH} and the initial AOB concentrations are given in Table S4 of the supplementary information. The affinity and inhibition constants for NH_3 and HNO_2 were taken from Van Hulle et al. (2007), because the biomass in our experiments was exposed to similar reactor conditions, and because it was close to the expected NH_3 affinity constant based on the analysis of the biomass (Section 4.3). All other growth parameters (Table 3) were taken from Jubany (2007) without further validating these values.

3.2. Conceptual metabolic model

Jin and Bethke (2002, 2007) proposed a rate law of the form:

$$r = r_+\cdot F_T \quad (8)$$

with r the net rate of the overall reaction (forward minus reverse rate), r_+ the forward reaction rate, and F_T the thermodynamic potential factor. Equation (8) is based on the concept that every chemical reaction can be written as a forward and reverse reaction, and that the equilibrium (r = 0) is reached once the forward and reverse reaction rates are in balance. During the dissolution and precipitation of minerals, for instance, this equilibrium is reached when the reaction's ion activity product Q and the equilibrium constant K are equal. In the electron transfer chain of bacteria the overall reaction rate becomes zero, if the energy stored in the

proton motive force just equals the energy required for ATP or NADH production.

F_T depends on the thermodynamic drive f, which can be expressed as:

$$F_T[-] = 1 - 10^{\left(-\frac{f}{\ln(10)\chi RT}\right)} \quad (9)$$

where f the thermodynamic driving force [J·mol^{-1}], χ a stoichiometric factor [−], R the universal gas constant [8.314 J·K^{-1}·mol^{-1}], and T the temperature [K]. The thermodynamic drive f can be expressed as:

$$f = mF\Delta p - \Delta G \quad (10)$$

where ΔG the Gibbs free energy change of the critical reaction in the electron transfer chain [J·mol^{-1}], m the protons translocated from the peri-to the cytoplasm [−], F the Faraday constant [96485 J·mol^{-1}·V^{-1}], Δp the proton motive force [V].

Aerobic bacteria transfer electrons from a substrate to O_2 through the electron transfer chain, during which protons are exported from the cyto- to the periplasm. The translocated protons result in a transmembrane electrochemical gradient: the proton motive force. The energy from the re-entry of protons from the peri- to the cytoplasm, (mFΔp) can then be used for the synthesis of ATP and NADH. If the energy from the re-entry of protons is far higher than the ΔG required for ATP or NADH synthesis then f is large and F_T approaches 1. However, F_T decreases to zero or to negative values as mFΔp is equal or below the ΔG required for ATP or NADH synthesis.

4. Results

4.1. pH limit of nitrification

Simulations of pH for all experiments are shown in Fig. 1. The pH value can be used directly to quantify the activity of AOB, because protons are released during ammonia oxidation. However, to be able to interpret the pH data quantitatively, the chemical speciation model must represent the effect of proton release on the pH value accurately. The chemical speciation model is discussed in Section 4.2.

Model 1 (Monod-type kinetics) is capable of representing pH values above pH 6, but the model completely fails to predict the course of the pH values below and the pH limit (Fig. 1, first row). Whereas the decrease in pH stops in the experimental data, the modeled pH keeps decreasing. In the model, it is not possible to stop the pH decrease by increasing the decay rate. Based on the model, biomass decay increases the pH, because the base NH_3 is released (Table 2). However the sharp bend in the pH curve close to the pH limit cannot be represented, even by adapting the decay coefficient (b_{AOB}). To fit the initial biomass concentrations only pH values between 7 and pH 5.8 for NH_4^+(a−e) and between 7 and 6 for NO_2^-(a−e) were used for Model 1. Fitting the whole pH range did not improve the poor ability of this model to represent the pH limit.

The modeled decrease in pH in Model 2 (Monod-type kinetics and sigmoidal pH term) is overestimated in the beginning and then underestimated (Fig. 1, second row). Between the pH values of 7 and 6, the course of pH can be fitted well, if no sigmoidal pH term is used (Model 1). In the latter case, the activity decrease is only due to NH_3 limitation at lower pH values. Including the sigmoidal pH term results in an overestimation of the pH effect. Model 2 also fails to predict a complete process stop. Fitting of the parameter pK in Model 2 (Table 3) does not improve the fit of the data.

Model 3 (Monod-type kinetics and exponential pH term) fits the data considerably better than Model 1 and 2 (Fig. 1, third row). Except from NH_4^+(a) and NH_4^+(b) Model 3 is also well suited to model the pH limit. In contrary to Model 2, the pH term in Model 3 affects the rate of AOB only at pH values below pH 6. In fact, this pH term decreases the rate of AOB sharply to zero as the pH limit is approaching. At pH values above pH 6 Model 3 is similar to Model 1. A value of 2.3 was fitted for K_{pH} in Model 3. The fitted initial biomass concentration for AOB were 0.09 ± 0.03 g COD·L^{-1} for Model 3 (Table S4, supplementary information), which is close to the AOB biomass concentration of 0.14 g COD·L^{-1} that can be calculated by assuming a biomass concentration of 1 g COD·L^{-1}, which was estimated for a similar reactor (Uhlmann, 2014), and a relative AOB abundance of 14% (Section 4.3).

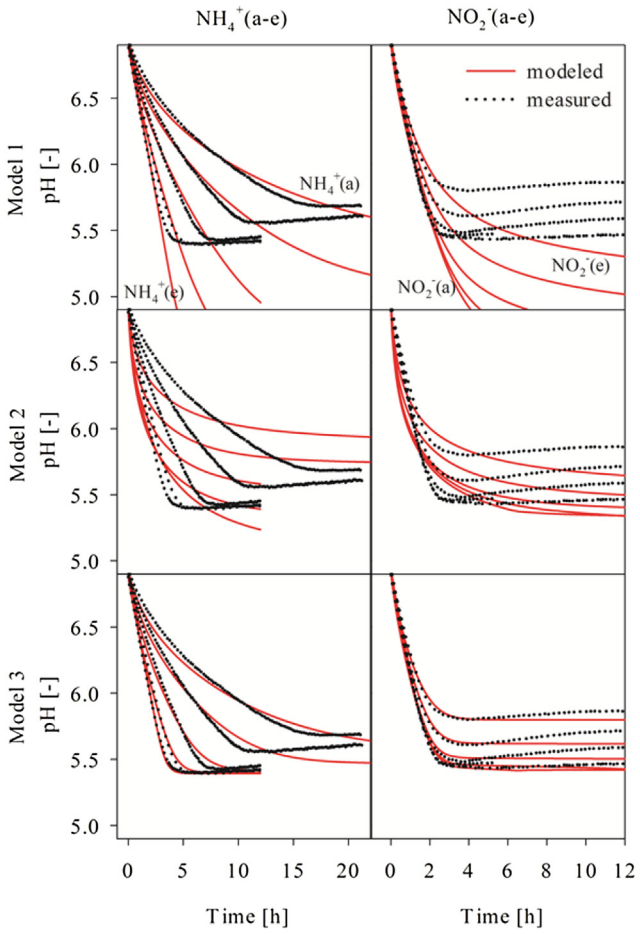

Fig. 1. Measured and simulated pH values for ten different experiments with synthetic solutions, the five experiments NH_4^+(a−e) containing different total ammonia concentrations and the five experiments NO_2^-(a−e) containing different total nitrite concentrations. Measured pH values (dotted) for NH_4^+(a−e) are depicted in all Figures of the left column, whereas the ones for NO_2^-(a−e) are depicted in the right column. Three models with different kinetic expressions for the growth of AOB were tested and model simulations for Model 1 to 3 are shown in row 1 to 3.

To model the pH limit of AOB in the experiments NO_2^-(a−e), we introduced a linear relationship for pH_{min} with the HNO_2 concentration (mol·L^{-1}):

$$pH_{min} = \frac{\{HNO_2\} + 0.002}{0.00037} \quad (11)$$

This relationship was introduced, because the HNO_2 concentrations and the pH limit showed a linear correlation (Fig. 2). This correlation was reproducible: a similar correlation was observed in four experiments in real nitrified urine with different amounts of

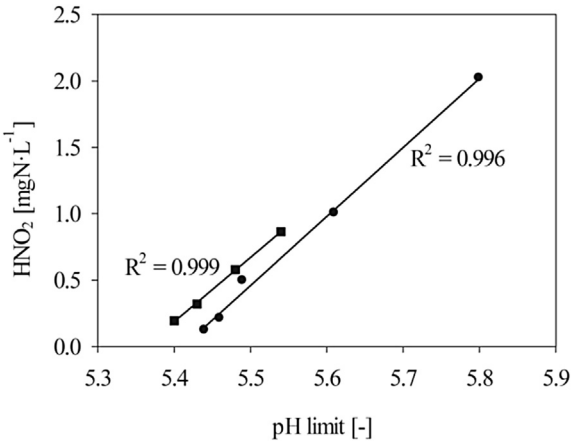

Fig. 2. Calculated concentrations of HNO_2 at the observed pH limit for *Nitrosomonas eutropha*. Each of the dots represents the endpoint of one experiment (■: experiments in real nitrified urine solutions, ● experiments in synthetic urine solutions).

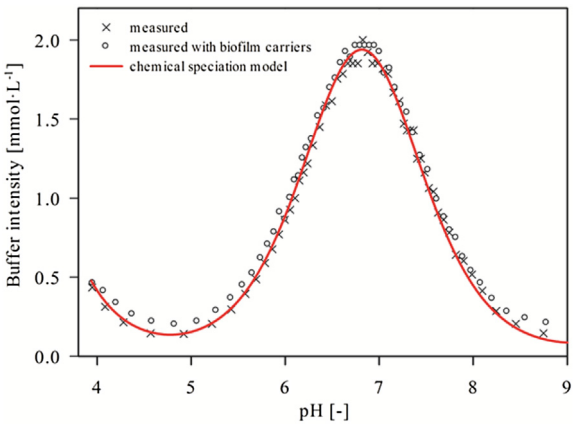

Fig. 3. Measured buffer intensity of a synthetic urine solution with phosphate as buffer system (NH_4^+(a), Table S1, supplementary information) with and without biomass. The line represents the model prediction.

nitrite added, and five experiments in synthetic nitrified urine (Fig. 2, Table S3 supplementary information).

The model was set up as a suspended growth model, but was applied for a biofilm system. At high conversion rates, e.g. at the beginning of the experiment NH_4^+(d) and NH_4^+(e), oxygen may have been limiting in the biofilm. However, oxygen limitation did not have an influence on the pH end-point (Figure S4, supplementary information), when ammonia conversion rates became very low. To prove that the model is not restricted to biofilm systems, we fitted experimental data from an experiment with suspended sludge with Model 3 with the same parameter set (except from the initial biomass concentration X_{AOB}, Figure S5, supplementary information). Also in this case Model 3 was suited to represent the measured data within the pH range of 7 to the pH limit. The experiment with suspended sludge was performed in a real nitrified urine solution, proofing that the model approach for AOB can be directly applied to real urine solutions.

The pH limit was also investigated at higher TIC concentrations. In two experiments with increased CO_2 in the aeration air the pH limit was at 5.36 (10% CO_2) and 5.37 (5% CO_2), which is only slightly lower than the pH limit observed at 5.46 in an experiment without CO_2 in the aeration (Table S3, supplementary information). Assuming an equilibrium of CO_2 between water and air phase, the TIC concentration would correspond to 23 and 46 mg $C \cdot L^{-1}$ for the aeration with 5 and 10% CO_2, respectively. This is far more than during the experiment with synthetic aeration without CO_2, where TIC concentrations were far below the detection limit (4 mg $C \cdot L^{-1}$). Due to the very different TIC concentrations at the pH limit, this parameter cannot explain the pH limit.

4.2. Chemical speciation model as basis for predicting pH

Titration experiments were performed to validate the chemical speciation model. A high reliability of the pH modeling was required, because pH was used to calculate the AOB activity in the batch experiments (Section 4.1). Fig. 3 shows the calculated and measured buffer intensity from a titration experiment with the synthetic urine solution NH_4^+(a) (Table S1, supplementary information). The buffer intensity ($\beta = dC_b/d\text{pH}$, with C_b the concentration of strong base in mol $\cdot L^{-1}$) describes the tendency of a solution at any point of the titration curve to change the pH upon addition of an acid or base (Stumm and Morgan, 1996). Modeled and observed buffer intensities correspond well, if acid-base equilibria, ionic strength and complex formation reactions are taken into account (Fig. 3 and Figure S1 to S3, supplementary information). An in-depth discussion of the model development is given in the supplementary information.

Besides dissolved compounds also biomass may act as a buffer (Batstone et al., 2012; Westergreen et al., 2012). However, the overall effect of biomass was low, which resulted in very similar measured buffer intensities in experiments with and without biofilm carriers (Fig. 3). To keep the complexity of the model low and to prevent the introduction of additional fitting parameters, we did not include biomass buffering into our model.

4.3. Characterization of the ammonium-oxidizing bacteria

According to the 16S rRNA gene-based amplicon pyrosequencing analysis conducted with the v1–v3 universal bacterial primers, the AOB populations present on the biomass carriers of the pilot scale reactor predominantly affiliated with the *Nitrosomonas europaea/Nitrosococcus mobilis* lineage. A relative abundance of 77% of the reads of the AOB guild affiliated with the *Nitrosomonas eutropha* strain C71 (GenBank acno. AAJE01000012) and strain C91 (GenBank acno. NC008344) as the closest cultured relatives with a sequence identity of 98%. AOB accounted for 14% of the overall bacterial community (corresponding to 3930 reads).

The high abundance of *Nitrosomonas eutropha* in urine is not surprising as *Nitrosomonas eutropha* are often selected in high salt and high ammonia environments. The affinity constant for ammonia ranges between 0.42 and 0.85 mg NH_3-$N \cdot L^{-1}$(Koops and Pommerening-Röser, 2001). The NH_3 affinity constant for NH_3 of 0.75 mg NH_3-$N \cdot L^{-1}$ that was used in the model simulations lies within this range (Van Hulle et al., 2007, Table 3).

5. Discussion

5.1. Bioenergetic considerations

The activity of AOB ceases, when the proton motive force is too small for ATP or NADH production (Section 3.2). NADH is required for many essential reductive biosynthesis pathways e.g., the capture of CO_2 (Ferguson et al., 2007), however, the production of NADH gets energetically more challenging at lower pH values (see below). The reduction of NAD^+ is coupled to the oxidation of ubiquinol (UQH_2) to ubiquinone (UQ), which can be written as:

$$NAD^+ + UQH_2 \rightleftharpoons NADH + UQ + H^+ \quad (12)$$

The ΔG° of this reaction is 113 kJ·mol^{-1} (25°C, Nicholls and Ferguson, 1997). According to equation (12), the actual Gibbs free energy change ΔG depends on the concentration ratios of NAD^+/NADH and UQ/UQH_2, respectively. Furthermore it depends on the intracellular pH, as protons are released to the cytoplasm during NADH production:

$$\Delta G = \Delta G^{\circ} + \ln(10)\cdot R\cdot T\cdot\left(\log\left(\frac{UQ\cdot NADH}{UQH_2\cdot NAD^+}\right) - pH_{in}\right) \quad (13)$$

It was experimentally observed for *Nitrosomonas europaea* that the intracellular pH decreases with the extracellular pH (Kumar and Nicholas, 1983). From the measured data in Kumar and Nicholas (1983), we derived a linear correlation for pH_{in} with pH_{out}:

$$pH_{in} = 0.6\cdot pH_{out} + 2.7 \quad (14)$$

Hence, as pH_{in} correlates with pH_{out}, the ΔG for NADH production will be higher and therefore energetically less favorable at lower extracellular pH values.

Equations (13) and (14) can be substituted into equation (9) to calculate the thermodynamic potential factor (equation (15)). This new equation depends on constants as well as on pH_{out}, which is similar to the pH term used in Model 3 (Presser et al., 1997):

$$F_T = 1 - 10^{\left(\frac{0.6}{\chi}\left(\frac{1}{0.6}\left(\frac{\Delta G^{\circ} - m\cdot F\cdot\Delta p}{\ln(10)\cdot R\cdot T} + \log\left(\frac{UQ\cdot NADH}{UQH_2\cdot NAD^+}\right) - 2.7\right) - pH_{out}\right)\right)}$$
$$= 1 - 10^{\left(K_{pH}\left(pH_{min} - pH_{out}\right)\right)} \quad (15)$$

from equation (15) K_{pH} and pH_{min} can be estimated as:

$$K_{pH} = \frac{0.6}{\chi} \quad (16)$$

and

$$pH_{min} = \frac{1}{0.6}\left(\frac{\Delta G^{\circ} - mF\cdot\Delta p}{\ln(10)\cdot R\cdot T} + \log\left(\frac{UQ\cdot NADH}{UQH_2\cdot NAD^+}\right) - 2.7\right) \quad (17)$$

To estimate K_{pH}, we assumed a stoichiometric coefficient χ of 0.248, as 0.248 mol of e^- are transferred from UQH_2 to NADH, when 1 mol of NH_3 is oxidized (Poughon et al., 2001). From equation (16), a K_{pH} of 2.4 can be estimated, which is almost identical to the fitted value of 2.3 in our experiments (Table 3).

To estimate pH_{min}, a proton motive force of 150 mV was assumed. This value was measured with little deviation for *Nitrosomonas europaea* over a wide pH range (Kumar and Nicholas, 1983). It was assumed that m corresponds to 4, as four protons re-enter the cytoplasm through the reversed complex I of the electron transfer chain in AOB, when 1 mol of NADH is produced (Poughon et al., 2001), which agrees with the current evidence that the proton translocation stoichiometry for complex I is $4H^+/2e^-$ (Nicholls and Ferguson, 1997). A pH_{min} of 5.4 can be estimated from equation (17), by assuming that NAD^+/NADH = 644 (Zhang et al., 2002) and UQ/UQH_2 = 0.1. The chosen NAD^+/NADH ratio of 644 is at the upper range of the reported NAD^+/NADH ratios (Lin and Guarente, 2003), whereas the estimated UQ/UQH_2 ratio of 0.1 is close to the reported minimal measured UQ/UQH_2 ratio of 0.25 in *Escherichia coli* (Bekker et al., 2007). Even though the exact concentration ratios are not known, it is thermodynamically consistent that the NAD^+/NADH ratio approaches a minimal and the UQ/UQH_2 a maximal ratio in order to keep the NADH production feasible as long as possible.

We observed in our experiments that pH_{min} increased with higher HNO_2 concentrations (Fig. 2). HNO_2, such as other small, uncharged molecules (e.g., lactic acid) penetrates the cell membrane, dissociates in the intracellular space and with that decreases the intracellular pH (Mortensen et al., 2008). A faster decrease in the internal pH decreases the thermodynamic feasibility of the NADH production (equation (13)) and causes a faster depletion of energy. Vice versa, if AOB keep the internal pH at higher levels, the thermodynamic feasibility of the NADH production would be increased, allowing for lower pH_{min}. It is known that acid-tolerant bacteria have mechanisms to keep their cell internal pH closer to neutrality than the external pH value (pH homeostasis) (Slonczewski et al., 2009). pH homeostasis could therefore be an important feature of acid-tolerant AOB (Gieseke et al., 2006; Udert et al., 2005) growing at pH values below pH 5.4.

It is stunning how well the fitted pH term (equation (3)) can be derived from bioenergetics principles, the general knowledge on energy metabolism in *Nitrosomonas europaea* and reported literature values. This is a strong indication that the pH limit observed for *Nitrosomonas eutropha*, which closely relates to *Nitrosomonas europaea*, is due to energy limitations connected to the proton transfer. For a complete proof of this concept, future studies should focus on the actual measurement of the parameter values that were taken from literature (e.g., proton motive force, intracellular pH, the concentration ratios of NAD^+/NADH and UQ/UQH_2).

5.2. Energy limitation

In previous studies it has been hypothesized that the pH limit of AOB is due to protein unfolding (Wiesmann et al., 2006), or membrane damage (Van Hulle et al., 2007). Low pH values can indeed compromise membrane stability and a prolonged decrease in the intracellular pH can lead to acid induced protein unfolding as well as DNA damages (Lund et al., 2014; Slonczewski et al., 2009). However, to prevent the detrimental effects of low intracellular pH values, most of the bacteria maintain a certain degree of pH homeostasis even in pH ranges, which do not allow for growth (Slonczewski et al., 2009). The pH range in which bacteria can survive without growth is therefore usually larger than the pH range where they can actually grow (Lund et al., 2014). Hence, it is unlikely that the pH limit of *Nitrosomonas eutropha* observed at a pH value close to 5.4 (Fig. 1) is due to membrane, protein or DNA damages. We also observed that that the nitrification rate recovered quickly as soon as the pH was increased (results not shown), which is in line with the theory that AOB are de-energized at the pH limit, but can be reactivated at higher pH values.

However, AOB were not reactivated if the pH increased only very slightly after reaching the pH limit (Fig. 1). We assume that the slight pH increase in the experiments is due to biomass decay. The pH increase was stronger for the experiments NO_2^-(a–e) than NH_4^+(a–e), which could be due to the increased HNO_2 concentrations: HNO_2 is known to increase the decay of activated sludge (Wang et al., 2013). Model 3 cannot represent this pH increase, because the rate of ammonia oxidation increases with the pH increase and returns the pH immediately back to the pH limit. In reality, however, it seems that such a small pH increase is not sufficient to reactivate the cell.

5.3. Implications for nitrification models

Nitrification of low buffered wastewaters is a very dynamic process, because the growth rate of AOB depends strongly on pH, but the pH is likely to change due to the low buffer intensity in these wastewaters. In urine, already small pH changes can outcompete NOB, which ends in an irreversible process failure as shown for laboratory reactors (Udert and Wächter, 2012) and pilot reactors (Etter et al., 2013). Nitrification models to describe such dynamic nitrification systems need therefore to accurately

represent (1) the pH itself (chemical speciation), and (2) the pH dependent growth rates.

Only a few studies set up nitrification models that include explicit pH calculations based on acid-base equilibria (e.g., Hellinga et al., 1999). However, the results of the current study show that at least the effects of ionic strength must be included for a realistic pH calculation in urine (Figure S1–S3, supplementary information), as well as in digester supernatant due to the similar ionic strength (e.g., 0.16 mol·L^{-1}, O'Neal and Boyer, 2013 compared to 0.1 mol·L^{-1} in the urine solutions of this study). In general, titration experiments are a powerful tool to investigate the accuracy and the degree of complexity that is required for the chemical speciation model.

To model the pH dependency of AOB different kinetic expressions have been developed. Hellinga et al. (1999) set up a model based on NH_3 limitation and HNO_2 inhibition only and calibrated this model for a pH range of 6.5–8.5. Our model simulations were in agreement with the model proposed by Hellinga et al. (1999): between pH 6 and 7, this model was sufficient to describe the ammonia oxidation in urine (Fig. 1). A direct pH term was only required at pH values below pH 6 in our simulations. This finding is in contrast with other studies for high strength nitrogen wastewaters, where sigmoidal or bell-shaped pH terms have been proposed (Antoniou et al., 1990; Claros et al., 2013; Jubany, 2007; Van Hulle et al., 2007). The pH terms in the latter studies decrease the rate of ammonia oxidation strongly between pH 7 and 6.

To investigate the influence of pH within a range of 5 to 9 and 6 to 9 respectively, Van Hulle et al. (2007) and Claros et al. (2013) used solutions with total ammonia concentrations between 500 and 1100 mgN·L^{-1}. It was assumed that this was sufficient to prevent any limitation of NH_3. However, considering an affinity constant of 0.75 mg N·L^{-1} (Van Hulle et al., 2007), limitation of NH_3 causes a decrease in AOB activity from 88% at pH 7 to 42% at pH 6 (25°C, 1000 mg NH_4-N·L^{-1}), which is very close to the observed drop in activity in Van Hulle et al. (2007) and Claros et al. (2013). Hence, limitation of NH_3 and not a pH inhibition can explain the observed activity drop.

After being able to model pH adequately and after successful implementation of the pH dependency of AOB in the urine nitrification model, future studies should focus on the calibration and validation of the further kinetic parameters used to model AOB and NOB growth in urine, e.g. the maximal growth rates (Table 3).

6. Conclusions

- *Nitrosomonas eutropha*, which are abundant in high strength nitrogen wastewaters show a pH limit close to 5.4. This limit and rates close to the limit cannot be explained or modeled with kinetics based on NH_3 and TIC limitation, or HNO_2 inhibition. Nitrification models based on Monod-type kinetics are therefore not suitable to understand and improve the process stability of nitrification reactors that are operated between pH 6 and the pH limit (e.g., nitrification reactors with urine). For reactors operated close to the pH limit, the reaction rate of AOB has to be extended by a direct pH term. The pH term decreases the rate of ammonia oxidation to zero as the pH drops below pH 6.
- The applied pH term bases on bioenergetic principles: as soon as the critical reaction in the electron transfer chain (NADH production) is thermodynamically not feasible, the growth rate becomes zero. This term might not only be suitable to model the low pH limit of *Nitrosomonas eutropha*, but for many other bacteria growing close to their thermodynamic pH limits.
- For nitrification reactors operated between pH 7 and 6 no additional pH term is required in the growth rate of AOB. The introduction of an additional pH term (e.g., as sigmoidal pH function) leads to an underestimation of the rate of ammonia oxidation, which is detrimental for the design of nitrification systems.

Acknowledgment

This study was funded by the Bill and Melinda Gates Foundation and was conducted as part of the VUNA project (www.vuna.ch, Grant No. OPP1011603). The authors like to thank Chris Brouckaert (Pollution Research Group, University of KwaZulu-Natal) for the helpful discussion about modeling chemical speciation. We also thank David G. Weissbrodt and George F. Wells for their help with the biomass analysis, Bastian Etter for setting up a pilot scale nitrification reactor, Karin Rottermann and Claudia Bänninger for the chemical analyses and Patrick Rambosson for the laboratory support.

Appendix A. Supplementary data

Supplementary data related to this article can be found at http://dx.doi.org/10.1016/j.watres.2015.06.013.

References

Altschul, S.F., Madden, T.L., Schaffer, A.A., Zhang, J., Zhang, Z., Miller, W., Lipman, D.J., 1997. Gapped BLAST and PSI-BLAST: a new generation of protein database search programs. Nucleic Acids Res. 25 (17), 3389–3402.

Anthonisen, A.C., Loehr, R.C., Prakasam, T.B., Srinath, E.G., 1976. Inhibition of nitrification by ammonia and nitrous acid. J. Water Pollut. Control Fed. 48 (5), 835–852.

Antoniou, P., Hamilton, J., Koopman, B., Jain, R., Holloway, B., Lyberatos, G., Svoronos, S.A., 1990. Effect of temperature and pH on the effective maximum specific growth rate of nitrifying bacteria. Water Res. 24 (1), 97–101.

Batstone, D.J., Amerlinck, Y., Ekama, G., Goel, R., Grau, P., Johnson, B., Kaya, I., Steyer, J.P., Tait, S., Takács, I., Vanrolleghem, P.A., Brouckaert, C.J., Volcke, E., 2012. Towards a generalized physicochemical framework. Water Sci. Technol. 66 (6), 1147–1161.

Bekker, M., Kramer, G., Hartog, A.F., Wagner, M.J., de Koster, C.G., Hellingwerf, K.J., Teixeira de Mattos, M.J., 2007. Changes in the redox state and composition of the quinone pool of *Escherichia coli* during aerobic batch-culture growth. Microbiology 153 (6), 1974–1980.

Claros, J., Jiménez, E., Aguado, D., Ferrer, J., Seco, A., Serralta, J., 2013. Effect of pH and HNO_2 concentration on the activity of ammonia-oxidizing bacteria in a partial nitritation reactor. Water Sci. Technol. 67 (11), 2587–2594.

DeSantis, T.Z., Hugenholtz, P., Larsen, N., Rojas, M., Brodie, E.L., Keller, K., Huber, T., Dalevi, D., Hu, P., Andersen, G.L., 2006. Greengenes, a chimera-checked 16S rRNA gene database and workbench compatible with ARB. Appl. Environ. Microbiol. 72 (7), 5069–5072.

Etter, B., Hug, A., Udert, K.M., 2013. Total nutrient recovery from urine – operation of a pilot-scale nitrification reactor. In: WEF/IWA Conference on Nutrient Removal and Recovery Vancouver, Canada.

Ferguson, S.J., Richardson, D.J., van Spanning, R.J.M., 2007. Chapter 14-biochemistry and molecular biology of nitrification. In: Hermann, B., Ferguson, S.J., William, E.N. (Eds.), Biology of the Nitrogen Cycle. Elsevier, Amsterdam, pp. 209–222.

Gieseke, A., Tarre, S., Green, M., de Beer, D., 2006. Nitrification in a biofilm at low pH values: role of *in situ* microenvironments and acid tolerance. Appl. Environ. Microbiol. 72 (6), 4283–4292.

Gustafsson, J.P., 2012. Visual MINTEQ Version 3.0, Royal Institute of Technology. Department of Land and Water Resources Engineering, Stockholm, Sweden.

Hellinga, C., Van Loosdrecht, M.C.M., Heijnen, J.J., 1999. Model based design of a novel process for nitrogen removal from concentrated flows. Math. Comput. Model. Dyn. Syst. 5 (4), 351–371.

Jin, Q., Bethke, C.M., 2002. Kinetics of electron transfer through the respiratory chain. Biophys. J. 83 (4), 1797–1808.

Jin, Q., Bethke, C.M., 2007. The thermodynamics and kinetics of microbial metabolism. Am. J. Sci. 307 (4), 643–677.

Jubany, I., 2007. Operation, Modeling and Automatic Control of Complete and Partial Nitrification of Highly Concentrated Ammonium Wastewaters. Universitat Autónoma de Barcelona, Bellaterra.

Koops, H.-P., Pommerening-Röser, A., 2001. Distribution and ecophysiology of the nitrifying bacteria emphasizing cultured species. FEMS Microbiol. Ecol. 37 (1), 1–9.

Kumar, S., Nicholas, D.J.D., 1983. Proton electrochemical gradients in washed cells of *Nitrosomonas europaea* and *Nitrobacter agilis*. J. Bacteriol. 154 (1), 65–71.

Lide, D.R., 2009. CRC Handbook of Chemistry and Physics, 89th ed. CRC Press/Taylor and Francis, Boca Raton, FL (Internet Version 2009).

Lin, S.-J., Guarente, L., 2003. Nicotinamide adenine dinucleotide, a metabolic regulator of transcription, longevity and disease. Curr. Opin. Cell Biol. 15 (2), 241–246.
Lund, P., Tramonti, A., De Biase, D., 2014. Coping with low pH: molecular strategies in neutralophilic bacteria. FEMS Microbiol. Rev. 38 (6), 1091–1125.
Mortensen, H.D., Jacobsen, T., Koch, A.G., Arneborg, N., 2008. Intracellular pH homeostasis plays a role in the tolerance of *Debaryomyces hansenii* and *Candida zeylanoides* to acidified Nitrite. Appl. Environ. Microbiol. 74 (15), 4835–4840.
Nicholls, D.G., Ferguson, S.J., 1997. Bioenergetics 2 (London).
O'Neal, J.A., Boyer, T.H., 2013. Phosphate recovery using hybrid anion exchange: applications to source-separated urine and combined wastewater streams. Water Res. 47 (14), 5003–5017.
Painter, H.A., 1986. Nitrification in the treatment of sewage and waste-waters. In: Prosser, J.I. (Ed.), Nitrification. IRL Press, Oxford, pp. 185–211.
Poughon, L., Dussap, C.-G., Gros, J.-B., 2001. Energy model and metabolic flux analysis for autrotrophic nitrifiers. Biotechnol. Bioeng. 72 (4), 416–433.
Presser, K.A., Ratkowsky, D.A., Ross, T., 1997. Modelling the growth rate of *Escherichia coli* as a function of pH and lactic acid concentration. Appl. Environ. Microbiol. 63 (6), 2355–2360.
Ratkowsky, D.A., 2002. Some examples of, and some problems with, the use of nonlinear logistic regression in predictive food microbiology. Int. J. Food Microbiol. 73 (2–3), 119–125.
Reichert, P., 1994. Aquasim – a tool for simulation and data-analysis of aquatic systems. Water Sci. Technol. 30 (2), 21–30.
Slonczewski, J.L., Fujisawa, M., Dopson, M., Krulwich, T.A., 2009. Cytoplasmic pH measurement and homeostasis in bacteria and archaea. Adv. Microb. Physiol. 55, 1–317.
Smith, R.M., Martell, A.E., Motekaitis, R.J., Standard Reference Data program (National Institute of Standards and Technology), 2004. NIST critically selected stability constants of metal complexes database, Version 8.0, Standard Reference Data Program. National Institute of Standards and Technology, U.S. Dept of Commerce, Gaithersburg, MD.
Stumm, W., Morgan, J.J., 1996. Aquatic Chemistry: Chemical Equilibria and Rates in Natural Waters. John Wiley & Sons Inc., New York.
Sun, Y., Wolcott, R., Dowd, S., 2011. Tag-encoded FLX amplicon pyrosequencing for the elucidation of microbial and functional gene diversity in any environment. In: Kwon, Y.M., Ricke, S.C. (Eds.), High-throughput Next Generation Sequencing. Humana Press, pp. 129–141.
Suzuki, I., Dular, U., Kwok, S.C., 1974. Ammonia or ammonium ion as substrate for oxidation by *Nitrosomonas europaea* cells and extracts. J. Bacteriol. 120 (1), 556–558.
Tchobanoglous, G., Burton, F.L., Stensel, H.D., Metcalf, E., 2003. Wastewater Engineering: Treatment and Reuse. McGraw-Hill, Boston.
Udert, K.M., Fux, C., Münster, M., Larsen, T.A., Siegrist, H., Gujer, W., 2003a. Nitrification and autotrophic denitrification of source-separated urine. Water Sci. Technol. 48 (1), 119–130.
Udert, K.M., Larsen, T.A., Gujer, W., 2003b. Estimating the precipitation potential in urine-collecting systems. Water Res. 37 (11), 2667–2677.
Udert, K.M., Larsen, T.A., Gujer, W., 2005. Chemical nitrite oxidation in acid solutions as a consequence of microbial ammonium oxidation. Environ. Sci. Technol. 39 (11), 4066–4075.
Udert, K.M., Wächter, M., 2012. Complete nutrient recovery from source-separated urine by nitrification and distillation. Water Res. 46 (2), 453–464.
Udert, K.M., Buckley, C.A., Wächter, M., McArdell, C.S., Kohn, T., Strande, L., Zöllig, H., Fumasoli, A., Oberson, A., Etter, B., 2015. Technologies for the treatment of source-separated urine in the eThekwini Municipality. Water SA 41, 212–221.
Uhlmann, C., 2014. Complete Nitrification of Urine. MSc thesis. ETH Zürich: Swiss Federal Institute of Technology, Zürich, Switzerland.
Van Hulle, S.W.H., Volcke, E.I.P., Teruel, J.L., Donckels, B., Van Loosdrecht, M.C.M., Vanrolleghem, P.A., 2007. Influence of temperature and pH on the kinetics of the Sharon nitritation process. J. Chem. Technol. Biotechnol. 82, 471–480.
Wang, Q., Ye, L., Jiang, G., Yuan, Z., 2013. A free nitrous acid (FNA)-based technology for reducing sludge production. Water Res. 47 (11), 3663–3672.
Weissbrodt, D.G., Shani, N., Sinclair, L., Lefebvre, G., Rossi, P., Maillard, J., Rougemont, J., Holliger, C., 2012. PyroTRF-ID: a novel bioinformatics methodology for the affiliation of terminal-restriction fragments using 16S rRNA gene pyrosequencing data. BMC Microbiol. 12.
Westergreen, S., Brouckaert, C.J., Foxon, K.M., 2012. Modelling of ionic interactions with wastewater treatment biomass. Water Sci. Technol. 65 (6), 1014–1020.
Wett, B., Rauch, W., 2003. The role of inorganic carbon limitation in biological nitrogen removal of extremely ammonia concentrated wastewater. Water Res. 37 (5), 1100–1110.
Wiesmann, U., Choi, I.S., Dombrowski, E.-M., 2006. Biological nutrient removal. In: Fundamentals of Biological Wastewater Treatment. Wiley-VCH Verlag GmbH & Co. KGaA, pp. 223–265.
Zhang, Q., Piston, D.W., Goodman, R.H., 2002. Regulation of corepressor function by nuclear NADH. Science 295 (5561), 1895–1897.